Improving the identification of hydrologically sensitive areas using LiDAR DEMs for the delineation and mitigation of critical source areas of diffuse pollution

Science of the Total Environment 556 (2016) 276–290

Contents lists available at ScienceDirect

Science of the Total Environment

journal homepage: www.elsevier.com/locate/scitotenv

Improving the identification of hydrologically sensitive areas using LiDAR DEMs for the delineation and mitigation of critical source areas of diffuse pollution

I.A. Thomas [a,b,*], P. Jordan [a,b], P.-E. Mellander [a], O. Fenton [c], O. Shine [a], D. Ó hUallacháin [c], R. Creamer [c], N.T. McDonald [a], P. Dunlop [b], P.N.C. Murphy [d]

[a] Agricultural Catchments Programme, Teagasc, Johnstown Castle, Wexford, Co., Wexford, Ireland
[b] School of Geography and Environmental Sciences, Ulster University, Coleraine, Northern Ireland, United Kingdom
[c] Teagasc, Environmental Research Centre, Johnstown Castle, Wexford, Co., Wexford, Ireland
[d] Environment and Sustainable Resource Management Section, School of Agriculture and Food Science, University College Dublin, Dublin 4, Ireland

HIGHLIGHTS

- A new HSA Index allows for mitigation of pollutant transfers.
- Flow sinks caused 17–33% of catchment areas to become hydrologically disconnected.
- HSA sizes were empirically estimated using rainfall-quickflow measurements.
- HSAs represented 2.9–8.5% of catchment areas during upper quartile storm events.
- Targeting riparian buffer strips at HSA delivery points would reduce costs.

GRAPHICAL ABSTRACT

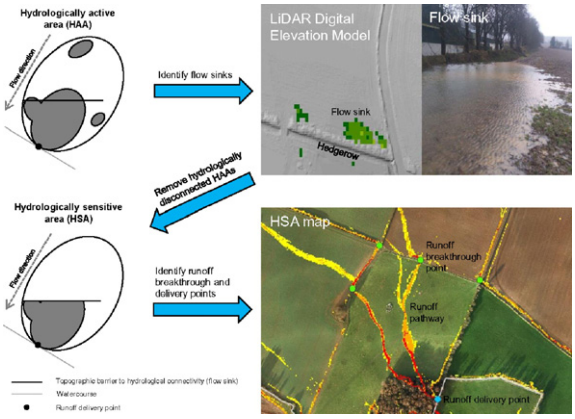

ARTICLE INFO

Article history:
Received 6 January 2016
Received in revised form 25 February 2016
Accepted 25 February 2016
Available online 12 March 2016

Editor: D. Barcelo

ABSTRACT

Identifying critical source areas (CSAs) of diffuse pollution in agricultural catchments requires the accurate identification of hydrologically sensitive areas (HSAs) at highest propensity for generating surface runoff and transporting pollutants. A new GIS-based HSA Index is presented that improves the identification of HSAs at the sub-field scale by accounting for microtopographic controls. The Index is based on high resolution LiDAR data and a soil topographic index (STI) and also considers the hydrological disconnection of overland flow via topographic impediment from flow sinks. The HSA Index was applied to four intensive agricultural catchments (~7.5–12 km^2) with contrasting topography and soil types, and validated using rainfall-quickflow measurements during saturated winter storm events in 2009–2014. Total flow sink volume capacities ranged from 8298 to 59,584 m^3 and caused 8.5–24.2% of overland-flow-generating-areas and 16.8–33.4% of catchment areas to

Abbreviations: CSA, critical source area; DEM, Digital Elevation Model; HAA, hydrologically active area; HSA, hydrologically sensitive area; LiDAR, Light Detection and Ranging; RBS, riparian buffer strip; SMD, soil moisture deficit; STI, soil topographic index; TWI, Topographic Wetness Index.

* Corresponding author.
E-mail addresses: ian.thomas@teagasc.ie (I.A. Thomas), p.jordan@ulster.ac.uk (P. Jordan), per-erik.mellander@teagasc.ie (P.-E. Mellander), owen.fenton@teagasc.ie (O. Fenton), oliver.shine@teagasc.ie (O. Shine), daire.ohuallachain@teagasc.ie (D. Ó hUallacháin), rachel.creamer@teagasc.ie (R. Creamer), noeleen.mcdonald@teagasc.ie (N.T. McDonald), p.dunlop@ulster.ac.uk (P. Dunlop), paul.murphy@ucd.ie (P.N.C. Murphy).

http://dx.doi.org/10.1016/j.scitotenv.2016.02.183

Keywords:
Hydrologically sensitive area
Critical source area
Diffuse pollution
LiDAR DEM
Agriculture
Mitigation

become hydrologically disconnected from the open drainage channel network. HSA maps identified 'breakthrough points' and 'delivery points' along surface runoff pathways as vulnerable points where diffuse pollutants could be transported between fields or delivered to the open drainage network, respectively. Using these as proposed locations for targeting mitigation measures such as riparian buffer strips reduced potential costs compared to blanket implementation within an example agri-environment scheme by 66% and 91% over 1 and 5 years respectively, which included LiDAR DEM acquisition costs. The HSA Index can be used as a hydrologically realistic transport component within a fully evolved sub-field scale CSA model, and can also be used to guide the implementation of 'treatment-train' mitigation strategies concurrent with sustainable agricultural intensification.

1. Introduction

Diffuse pollution from agricultural land to waterbodies has been identified as a major cause of eutrophication and water quality degradation worldwide (Jarvie et al., 2013; Daniel et al., 1998), with mitigation measures part of wide ranging and international environmental policies (Schoumans et al., 2014; Mcdowell and Nash, 2012; Murphy et al., 2015). Catchment areas at highest transfer risk of pollutants are termed critical source areas (CSAs) and are often identified as land use conflict areas (Valle Junior et al., 2014). More specifically, CSAs are where pollutant sources coincide with areas of high mobilisation potential and hydrologically sensitive areas (HSAs) that have the highest propensity for surface runoff generation, pollutant transport and delivery via hydrologically connected pathways (Pionke et al., 2000; Walter et al., 2000; Agnew et al., 2006) (Fig. 1). HSAs are a water quality concept relating saturation-and-infiltration-excess mechanisms of overland flow generation and hydrological connectivity concepts to associated pollutant transport, delivery and CSAs (Fig. 1; Walter et al., 2000; Agnew et al., 2006). They must be accurately identified if mitigation measures and best management practices aimed at reducing or offsetting diffuse pollution are to be cost-effectively designed and targeted (Sharpley et al., 2011; Doody et al., 2012).

Recent research has demonstrated the importance of accurately identifying HSAs when identifying and mitigating CSAs. Catchment hydrology has been found to be an important part of CSAs of phosphorus transfers in agricultural catchments (Campbell et al., 2015; Ulén et al., 2007; Heckrath et al., 2008; Shore et al., 2014). In some of these studies, HSAs were a dominant CSA factor which outweighed source and land management pressures (Jordan et al., 2012; Buda et al., 2009; Mellander et al., 2015; Needelman et al., 2004; Kleinman et al., 2011; Fig. 1). Catchment areas were hydrologically sensitive to rainfall because of the prominence of poorly drained soils (with low permeability and/or infiltration capacity), or impermeable subsurface soil layers such as fragipans that caused perched water tables. Such findings are consistent with the concept of the pollutant transfer continuum (Haygarth et al., 2005; Lemunyon and Gilbert, 1993), whereby pollutant sources are only delivered to receiving waters if transport pathways exist (Fig. 1).

In certain CSA definitions, watercourse proximity is typically used as a proxy of runoff propensity (Lemunyon and Gilbert, 1993; Gburek et al., 2000; Sharpley et al., 2003; Srinivasan and Mcdowell, 2007). Land adjacent to watercourses is assumed to be a HSA, and as such is considered a CSA if source pressures exist (Campbell et al., 2015; Gburek et al., 2000). This approach is convenient for implementing measures within agricultural policy, and is the basis of riparian buffer

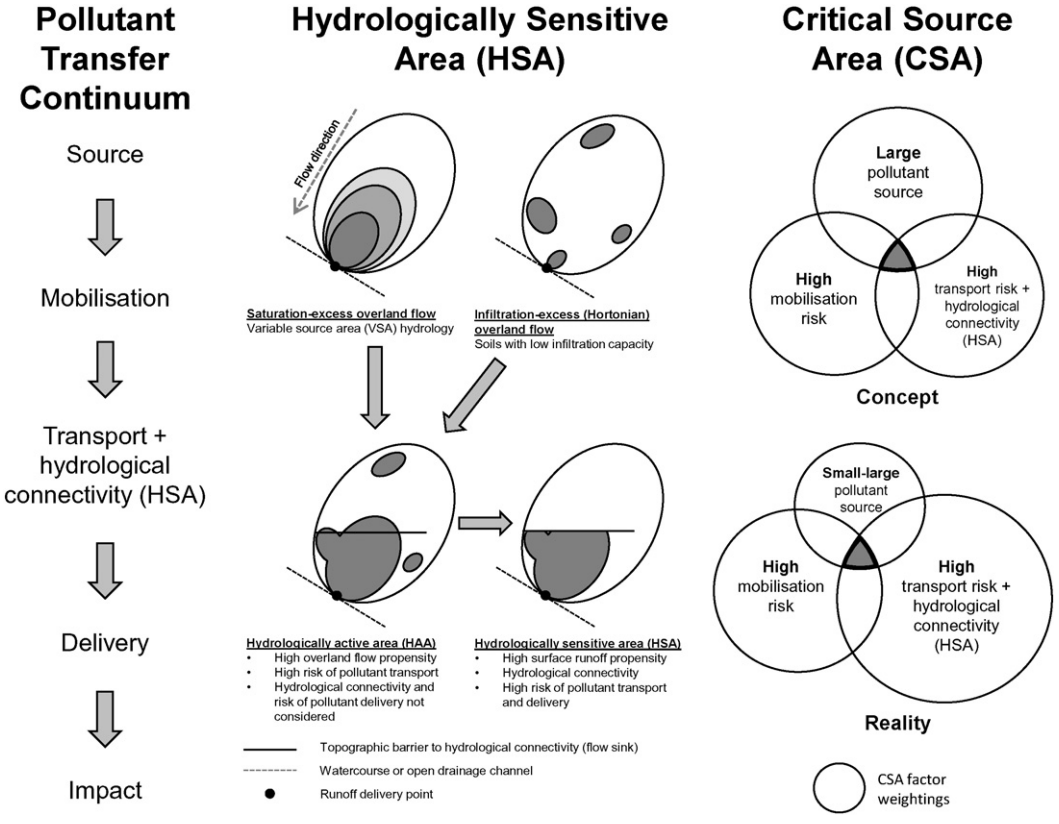

Fig. 1. Conceptual diagram of pollutant transfer continuum (adapted from Haygarth et al., 2005), HSAs and CSAs (adapted from Agnew et al., 2006).

strip (RBS) measures which, from a water quality point of view, are designed to impede surface runoff and reduce pollutant delivery. However, the approach is also an extreme simplification of reality, as overland flow tends to channelise and converge due to topographic and microtopographic influences (Thomas et al., 2014; Marjerison et al., 2011; Qiu, 2003) and does not always flow uniformly downslope as a sheet (Ó hUallacháin, 2014; White and Arnold, 2009). Thus some CSA definitions overestimate the size of the HSA at the stream and underestimate HSAs upslope, and hence poorly define pollutant transport potential in surface runoff (Sharpley et al., 2013; Srinivasan and Mcdowell, 2009).

More scientifically robust approaches to delineating HSAs include topographic indices which use Digital Elevation Models (DEMs), such as the Topographic Wetness Index (TWI) by Beven and Kirkby (1979). It is defined as $TWI = \ln(\alpha / \tan\beta)$, where α is the cumulative upslope drainage area per unit contour length and $\tan\beta$ is the surface slope gradient. Larger upslope drainage areas and shallower slopes will produce larger TWI values which indicate higher runoff propensity (Quinn et al., 1991). A modification called the soil topographic index (STI) also accounts for the soil water storage capacity, and is defined as $STI = \ln(\alpha / \tan\beta) - \ln(K_s D)$, where D is the local soil depth in metres to the restrictive layer (e.g. bedrock or fragipan) and K_s is the mean saturated hydraulic conductivity of the soil profile in metres per day above the restrictive layer (Walter et al., 2002). Shallower soils and those with lower saturated hydraulic conductivities will have lower soil water storage capacities and higher runoff propensities. Thus the approach accounts for hydrological disconnection of overland flow from the open drainage channel network due to reinfiltration at unsaturated soils which have larger soil water storage capacities. Topographic indices have been found to improve predictions of soil moisture, HSAs and pollutant loads from diffuse sources compared to approaches that do not consider topography, such as watercourse proximity (Buchanan et al., 2014; Agnew et al., 2006; Hahn et al., 2014).

However, topographic indices such as the TWI or STI do not consider the hydrological disconnection of overland flow from topographic impediment within flow sinks such as depressions, hummocks, hedgerow banks or other microtopographic features. Thus they do not differentiate between hydrologically active areas (HAAs; overland-flow-generating-areas) and HSAs (runoff-generating-areas). This is because topographic indices are typically derived from hydrologically corrected DEMs which remove (fill) all flow sinks so that flow pathways are continuous and hydrologically connected to the catchment outlet (Jenson and Domingue, 1988; Maune et al., 2007). This improves the modelling of subsurface and groundwater flow pathways and associated propensity for overland flow generation. However, removing flow sinks incorrectly assumes that all of these features do not exist, and are a result of DEM vertical error (Lindsay and Creed, 2006; Wechsler, 2007). In fact many flow sinks are real topographic features which have important influences on the pathways and hydrological connectivity of overland flow once it is generated (Li et al., 2011; Lane et al., 2009). This is important because once overland flow is impeded, it will reinfiltrate and deposit and immobilise dissolved or entrained pollutants, and hence the upslope drainage area will not be a HSA or CSA (Fig. 1). These microtopographic features often dominate agricultural catchments, and must be considered when identifying HSAs/CSAs and targeting mitigation measures as they could represent existing mitigating features in the landscape (Thomas et al., 2014; Sherriff et al., 2015).

High resolution DEMs with high vertical accuracies derived from Light Detection and Ranging (LiDAR) technology can now accurately capture these microtopographic flow sinks (Maune et al., 2007; Lindsay and Creed, 2006; Li et al., 2011). Furthermore, they allow modelling of HSAs and CSAs at optimal resolutions, accounting for microtopographic controls on surface runoff pathways, hydrological connectivity and soil erosion (Vaze et al., 2010; Djodjic and Villa, 2015; Galzki et al., 2011; Petroselli, 2012). As such, breakthrough points and delivery points along surface runoff pathways where pollutants are transported between fields or delivered to the open drainage network, respectively, can now also be accurately identified (Thomas et al., 2014). LiDAR DEMs could therefore significantly improve the identification of HSAs and targeting of mitigation measures such as RBS within agricultural policies to reduce diffuse pollution from CSAs.

To improve the identification of HSAs, in order to accurately delineate CSAs of diffuse pollution and target mitigation measures, this study had three objectives: (1) to develop a GIS-based HSA Index which uses LiDAR DEMs and the STI, and accounts for hydrological disconnection of overland flow via topographic impediment from flow sinks; (2) to validate the HSA Index using rainfall-quickflow measurements; (3) to identify cost-effective locations at identified HSAs where sub-field scale diffuse pollution mitigation measures such as RBS could be targeted.

2. Materials and methods

2.1. Study sites and deriving STI maps

Four agricultural catchments in Ireland were selected for this study (Fig. 2). Catchment details are fully described elsewhere (Wall et al., 2011; Jordan et al., 2012; Shore et al., 2013), and the main hydrophysical details are summarised in Table 1.

To derive TWI and STI maps, 2 m resolution LiDAR DEMs were utilised (Supplementary Fig. 1). These represented optimal grid resolutions for modelling flow pathways in catchments dominated by microtopography, and were resampled from 0.25 m resolution LiDAR DEMs with horizontal and vertical accuracies of 0.25 m and 0.15 m, respectively (Thomas et al., 2014). A multi-step method (work-flow described in Supplementary Fig. 2) was used to hydrologically correct DEMs and derive TWI maps. DEMs were hydrologically corrected in SAGA GIS v.2.1 by 'burning' a field-mapped open drainage channel network into the DEM. To model fully connected flow pathways to the catchment outlets, flow sinks were identified and filled using the method for LiDAR datasets by Wang and Liu (2006). The Deterministic Infinity method by Tarboton (1997) was used to model multiple flow directions and upslope drainage areas, and slope was modelled using the method by Zevenbergen and Thorne (1987). To derive STI maps, soil subgroup maps from the Irish Soil Information System (Creamer et al., 2014) were imported into ArcGIS v10.0 and improved using additional soil sampling, expert knowledge and the DEMs. The dominant soil series for each soil subgroup was identified based on these data and assigned to each soil subgroup. The Irish Soil Information System was then used to extract soil series properties used for D (soil depth) and K_s (soil texture, bulk density and soil horizon thickness). A pedotransfer function was used to determine bulk densities of soil horizons where data were unavailable (Reidy et al., 2016). K_s values were calculated using the Retention Curve model (van Genuchten et al., 1991), and a $\ln(K_sD)$ raster was then created. As texture, and hence K_sD, is not determinable for peat soils, a K_sD value of 0.083 was assigned which was the equivalent value of the Kilrush soil series (Typical Surface-water Gley) (R. Creamer, pers comm). Similarly, roads identified using orthophotos were assigned an arbitrary K_sD value of 0.002, representing their impermeability and high runoff risk. Other linear features such as farm tracks and wheelings were not considered due to variability in permeability, location and lack of information. Also, although subsurface artificial drainage may increase K_s, this was not considered in this study, as field surveys of drainage ditches suggest few exist in these catchments, and high variability may exist in their design, age and effectiveness. An STI map was then created by subtracting the $\ln(K_sD)$ raster from the TWI raster using the raster calculator tool.

2.2. Empirically estimating HSA sizes using rainfall-quickflow measurements

To validate the HSA Index, high resolution rainfall-quickflow measurements from 2009 to 2014 were used to empirically estimate the

size of runoff-generating-areas (HSAs) during storm events in each catchment. Daily rainfall depths were calculated from gauging stations within the catchments. Quickflow volumes were estimated by separating hydrographs of hourly discharge (measured at 10 minute intervals from automatic gauging stations at catchment outlets), using a graphically interpreted hydrograph separation method described by Mellander et al. (2012, 2015). Although quickflow volumes were likely a sum of surface runoff, preferential flow and tile and ditch drainage, all quickflow was assumed to be surface runoff in this study. This assumption was supported from field surveys of the drainage ditches within the study catchments which showed little evidence of subsurface drainage. The Soil Moisture Deficit (SMD) model by Schulte et al. (2005) was used to calculate daily SMDs for each soil drainage class for the same period using meteorological data. Quickflow events were selected during winter and spring months on days with saturated conditions (i.e. ≤0 mm SMD depending on the soil drainage class), when saturation-excess (and potentially infiltration-excess) HSAs would become most active. To minimise noise from old water contributions (i.e. time lag; Fenton et al., 2011), only events that were not preceded by heavy rainfall/quickflow were selected. For each selected event, the daily quickflow volume (m^3) was divided by the daily rainfall depth (m) to estimate the HSA size (m^2) generating the observed quick flow (runoff) volume. The HSA size as a proportion of the catchment was then calculated for median, lower quartile (LQ) and upper quartile (UQ) rainfall-quickflow events.

2.3. Developing the HSA Index by accounting for flow sinks

An HSA Index (dimensionless) was developed by modifying the STI to account for the effects of flow sinks on hydrological connectivity of overland flow. This modification involved reducing STI values in upslope drainage areas of flow sinks large enough to topographically impede and trap overland flow generated within an UQ storm event (method shown in Supplementary Fig. 2). To do this, flow sinks were extracted from the DEM, and their depth and area used to calculate their overland flow volume capacity. These sink maps were derived from 0.25 m LiDAR DEMs to improve accuracy and then resampled to 2 m grid resolutions to optimise modelling of flow sink upslope drainage areas and reduce computational demands. Flow sinks within lakes and the open drainage channel network were removed as they were assumed hydrologically connected to the catchment outlet. Very small flow sinks (<0.05 m depth and <1 m^3 volume capacity) were also removed as they would likely have a negligible effect on impeding overland flow and could also represent DEM vertical error (flow sinks < 1 m^3 numbered between 2772 and 7782).

To calculate the overland flow volume generated within the flow sink upslope drainage area, the size of the HAA had to be known. The proportion of the catchment which was an HAA during an UQ storm event was estimated by arbitrarily increasing the UQ HSA size (estimated from rainfall-quickflow data) by 20%. The HAA was spatially distributed within the catchment by selecting the catchment areas with the

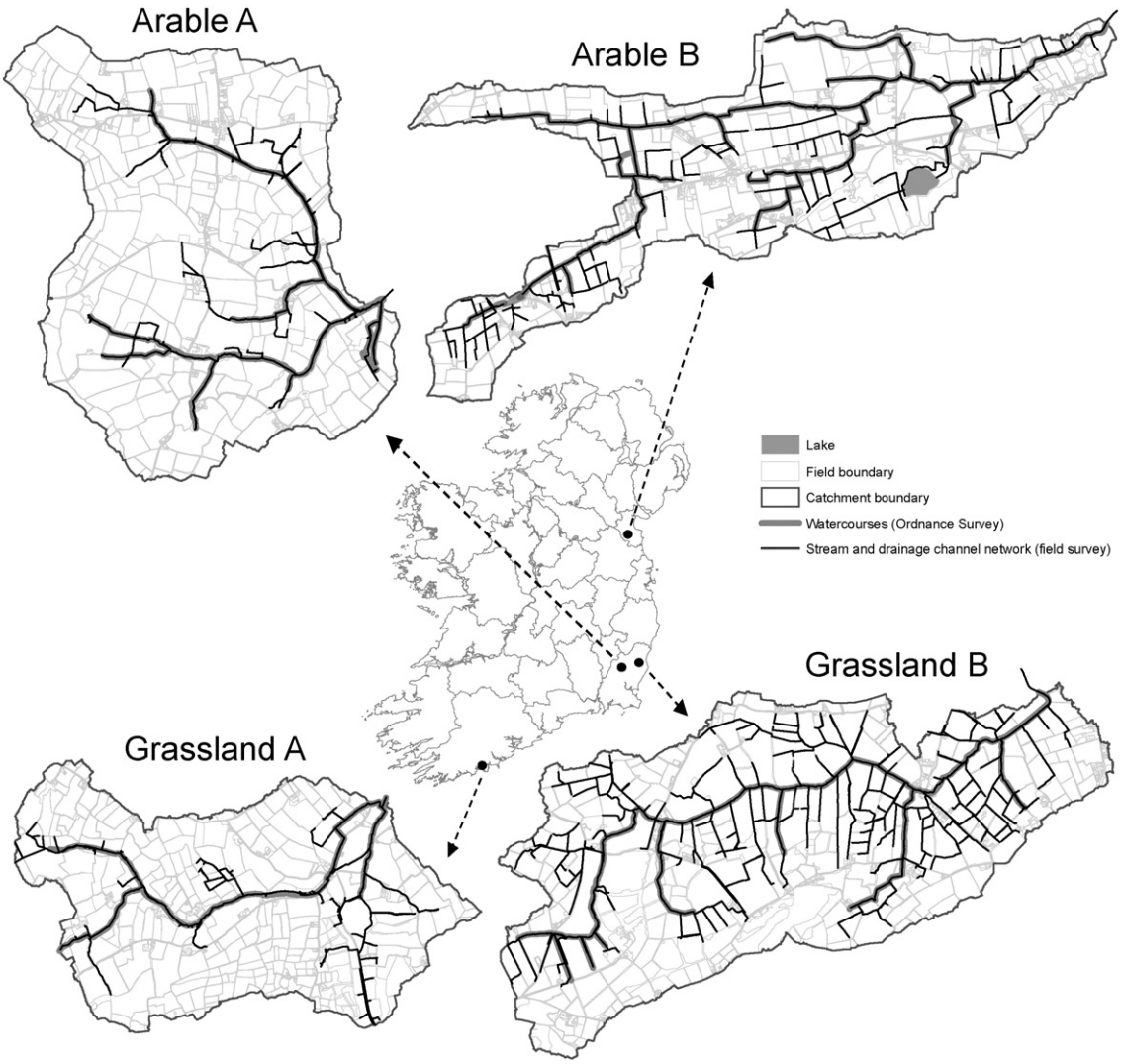

Fig. 2. Locations of the agricultural catchments in Ireland used in the study.

Table 1
Catchment characteristics.

	Arable A	Arable B	Grassland A	Grassland B
Area (ha)	1116	948	758	1207
Land use	Arable (54%) Grassland (39%)	Arable (33%) Grassland (49%)	Arable (6%) Grassland (84%)	Arable (20%) Grassland (77%)
Soil drainage class	Well drained soils	Mixture of well, moderately, imperfectly and poorly drained soils	Well drained soils	Poorly drained soils Well drained soils in uplands
Dominant soil types	Typical Brown Earths (88%), Gleyic Brown Earths (5%), Typical Groundwater Gleys (5%)	Stagnic Brown Earths (35%), Typical Surface-water Gleys (25%), Typical Brown Earths (22%)	Typical Brown Earths and Typical Brown Podzols (84%), Typical Surface-water Gleys (5%), Humic/Typical Alluvial Gleys (4%)	Typical Surface-water Gleys or Groundwater Gleys (71%) Typical Brown Earths (29%)
Dominant hydrological pathway for storm flow	Subsurface	Surface and subsurface	Subsurface	Surface and subsurface
Average annual rainfall (mm) from 2010 to 2014 hydrological years	1021	913	1117	1078
Geology	Slate and siltstone	Calcareous greywacke and mudstone	Sandstone, mudstone and siltstone	Rhyolitic volcanic and slate

highest STI values until the catchment area selected was the HAA size. The lowest STI value within this selection was identified as the STI threshold value for delineating HAAs.

To calculate the overland flow volume generated from the HAA within the flow sink upslope drainage area, the HAA size (m^2) was multiplied by the UQ rainfall depth (m) to calculate the overland flow volume (m^3). If the overland flow volume was less than the flow sink volume capacity, the flow sink would topographically impede the overland flow and not 'fill and spill', and the whole upslope drainage area would by hydrologically disconnected from the open drainage network.

The HSA Index was created by reducing STI values within these hydrologically disconnected flow sink upslope drainage areas by 75%. Thus high STI values (HAAs) within these areas were now low HSA Index values and not considered as HSAs. HSAs were spatially distributed within the catchment by selecting the catchment areas with the highest HSA Index values up to the same STI threshold value used to delineate HAAs. If the catchment area selected was larger or smaller than the UQ HSA size estimated from rainfall-quickflow data, the HAA size (originally estimated as 20% larger than the HSA size) was refined and the processes repeated. HSA maps for UQ as well as LQ and median storm events were then created.

2.4. Validating the HSA Index

Value distributions of slope, upslope drainage area, TWI, STI, flow sink depth (≥ 0.05 m), flow sink volume capacity (≥1 m^3) and the HSA Index were analysed for each catchment. The HSA Index was validated by comparing the HSA size predicted by HSA Index threshold values with the HSA size estimated by the rainfall-quickflow data using correlation analysis. A range of HSA Index threshold values were tested, from the lowest threshold value which matched the observed HSA size of a catchment, to the highest. Thresholds ranged from 13.3–14.7 for LQ storm events, 11.9–12.8 for median storm events, and 10.9–11.7 for UQ storm events. The same correlation analysis was repeated for the STI using the same threshold values for comparisons in performance of the two indices.

2.5. Using HSA maps to identify cost-effective locations for targeting mitigation measures

HSA maps were used to identify breakthrough points and delivery points at HSAs as these were deemed to be cost-effective locations for targeting diffuse pollution mitigation measures if source pressures existed at present or in the future. These locations were prioritised based on the size of the upslope HSA draining into that point (a similar concept to upslope drainage area) and whether it would become active during LQ, median or UQ storm events. Furthermore, the costs of targeted and blanket implementation approaches over 1 and 5 years were estimated for each catchment using the RBS measure from the current agri-environment scheme in Ireland (Green Low-carbon Agri-environment Scheme, GLAS; DAFM, 2015) as a case study. This is a realistic comparison as current RBS policies and the HSA approach here are based on hydrological risk only and do not consider pollution sources as in fully evolved CSAs. The total RBS length was calculated along the whole field-mapped open drainage channel network for the blanket approach, and at HSA delivery points for the targeted approach. RBS establishment costs were derived from current GLAS payment rates (€/m/yr) for each of the four margin widths available (3, 6, 10 and 30 m). These generic RBS establishment costs are included for case-study comparisons only and do not take into account likely variations in costs associated with establishing RBS in arable and grassland systems. The costs of the targeted approach also included an additional one-off cost of acquiring a LiDAR DEM for a 10 km^2 size catchment which ranged from €10,000–40,000, based on Ó hUallacháin (2014) and this study. Costs of targeted and blanket implementation of RBS were then compared.

3. Results

3.1. STI, flow sinks and HSA sizes

STI and flow sink maps are shown in Fig. 3a and b. Distributions of values of slope, upslope drainage area, TWI and STI are shown in Fig. 4. Due to the high resolution (2 m) LiDAR DEMs used, individual surface flow pathways are clearly identifiable. A larger proportion of Grassland B had higher STI values (i.e. ≥10) compared to the other catchments due to the dominance of poorly drained soils with low K_sD values (see Supplementary Fig. 3a and b). This was despite it having the lowest TWI value distributions due to small upslope drainage areas from a dense drainage network. Conversely, Arable A had the highest TWI distributions due to large upslope drainage areas, but the lowest STI values (with Grassland A) due to the dominance of well drained soils with high K_sD values. Arable B, which has a mixture of soil drainage classes, showed a larger proportion of high STI values compared to well drained Arable A and Grassland A. High STI values in these latter catchments tended to be found in concentrated areas where more imperfectly or poorly drained soils existed, particularly in lower hillslope positions.

Daily rainfall, quickflow and SMD data (for well drained soils) during 2009–2014 for each catchment are shown in Fig. 5. Grassland B had

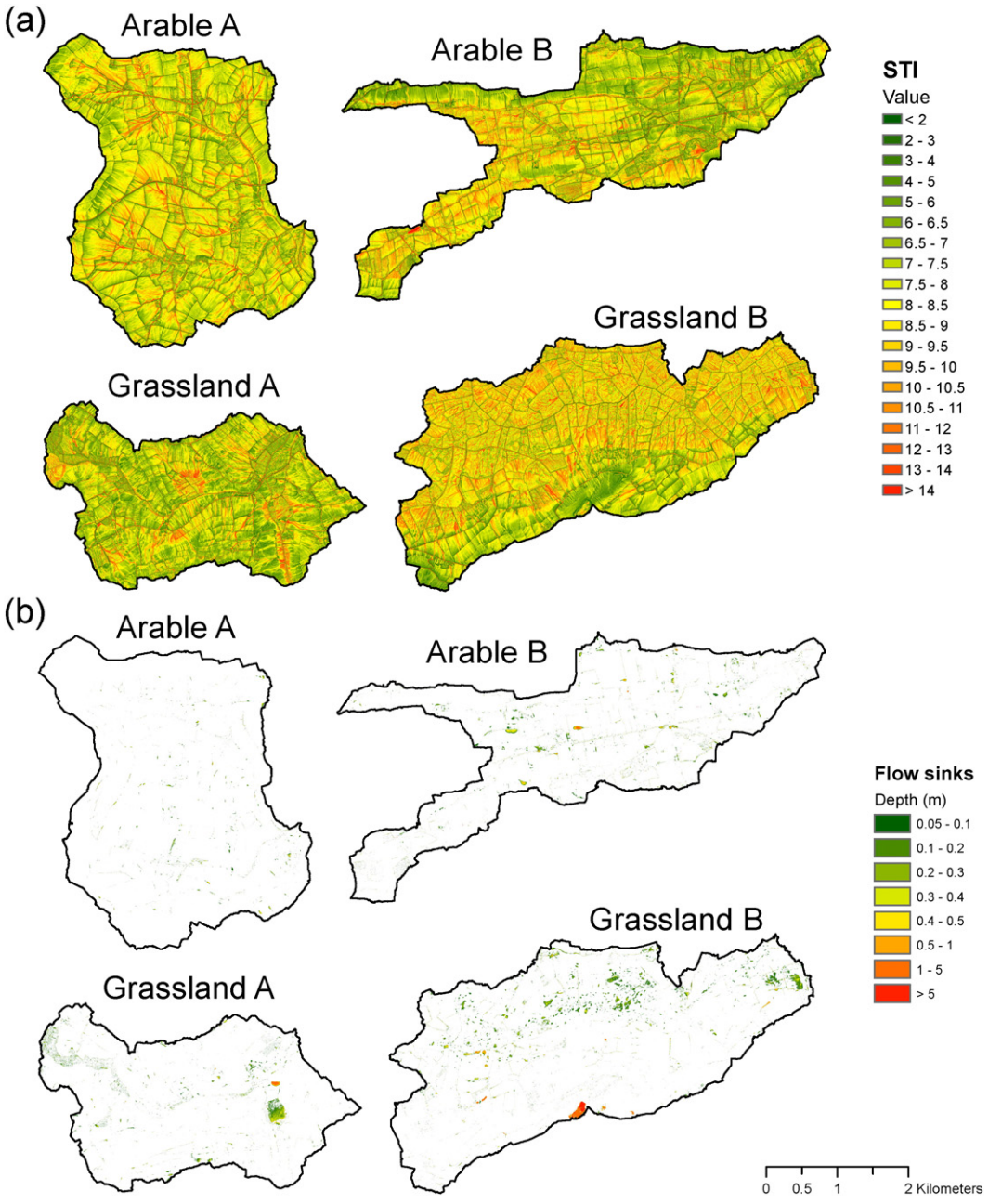

Fig. 3. Maps of the STI (a) and flow sinks (b) for each catchment.

much larger, flashier and more frequent runoff events, followed by Arable B. Arable A and Grassland A showed similar rainfall-quickflow responses, which were the lowest magnitudes of the four catchments. Arable A also showed more prolonged periods of elevated quickflow following rainfall, indicating old water contributions (i.e. not quickflow) and time lag dynamics. All catchments showed broadly similar magnitudes and temporal dynamics of rainfall and SMD, reflecting the dominant influence of North Atlantic weather systems.

HSA sizes as a proportion of each catchment, estimated using the rainfall-quickflow data for selected events during saturated conditions, are shown in Table 2. HSA sizes during LQ, median and UQ events were similar for Arable A and Grassland A, and represented relatively small proportions of the catchment (≤3.2%). However, during the largest rainfall-quickflow events, HSA sizes represented significant catchment proportions (6.2–15.1%). Although LQ-median events in Grassland B also indicated relatively modest HSA sizes (2.1–3.4%), UQ and maximum sizes (8.5% and 19.1%, respectively) demonstrate the hydrological sensitivity of this catchment. HSA sizes in Arable B were the second highest of the four catchments.

For each catchment, Table 3 shows the total number of flow sinks, the total flow sink volume capacity, and the proportion of HAAs and catchment area that are hydrologically disconnected. Flow sinks were found throughout all catchments and represented very large overland flow volume capacities (between 8298 and 59,584 m^3). Thus these features were found to be significant barriers to hydrological connectivity of overland flow in all catchments, particularly in Arable B and Grassland A and B, causing up to 24.2% of HAAs and 33.4% of catchment areas to become hydrologically disconnected.

3.2. HSA maps

HSA Index and specific HSA location maps during upper, median and lower quartile storm events for each catchment are shown in Fig. 6a and b, respectively. Maps of HSAs indicate that all catchments experience

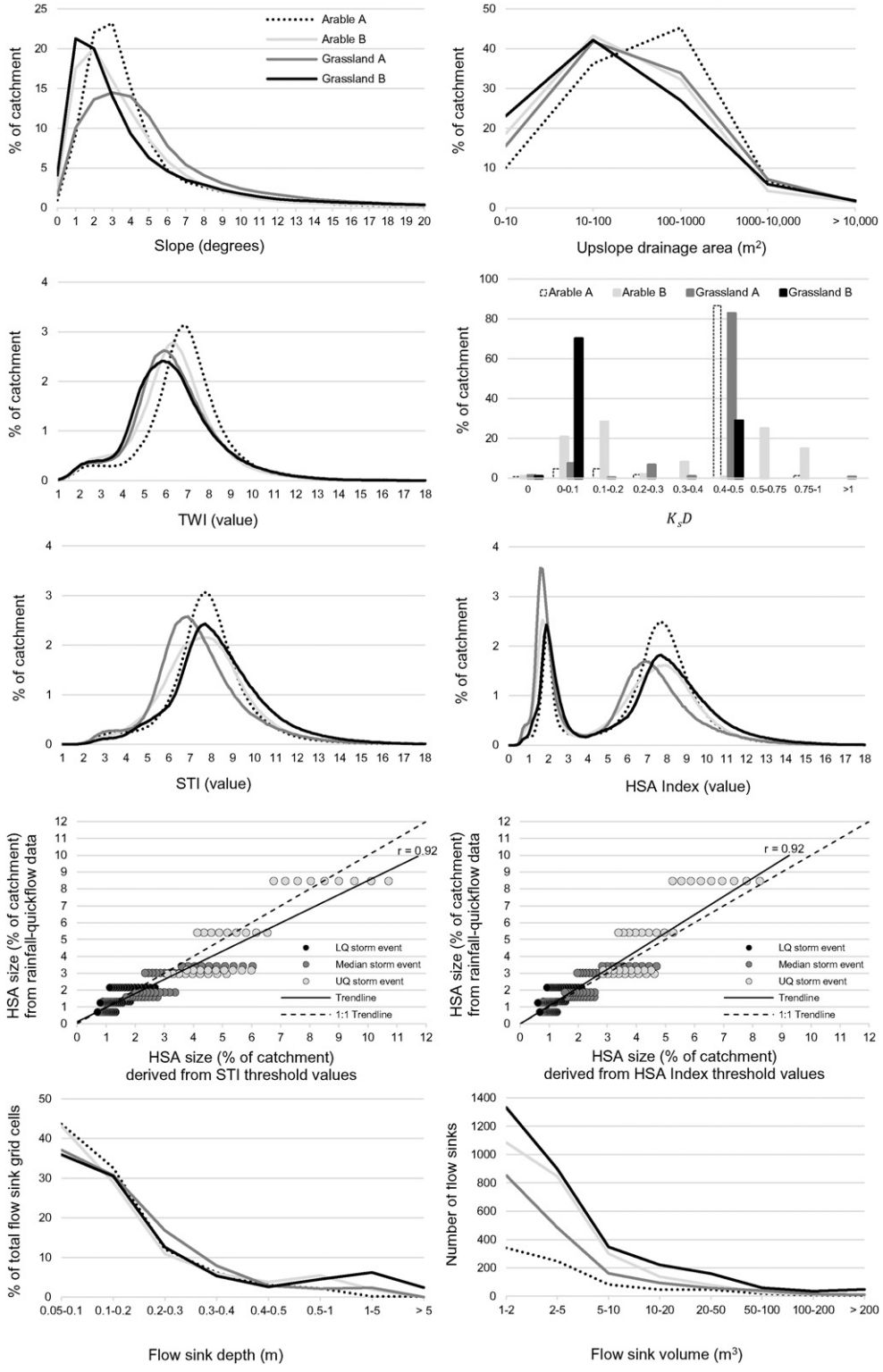

Fig. 4. Distributions of values of slope, upslope drainage area, TWI, STI, HSA Index, flow sink depths (≥0.05 m) and flow sink volumes (≥1 m^3) for each catchment. Correlation analysis between the proportion of the catchment predicted to be an HSA using the STI or HSA Index and the proportion estimated using rainfall-QF data is also shown.

both channelised and uniform sheet flow of runoff (including within riparian margins) because each catchment had a mixture of concave and convex hillslope topography. However, HSAs were much more diffuse and complex in Grassland B due to a combination of complex, hummocky microtopography (see Supplementary Fig. 1) and the dominance of poorly drained soils with low K_sD across the catchment (see Supplementary Fig. 3b). HSAs in Arable A and Grassland A were typically confined to poorly drained areas in lower hillslope positions, although narrow pathways also extended into upper hillslope positions. HSAs in Arable B were typically channelised, and situated in the imperfectly and poorly drained soils in the East, South and South-West. Within all catchments, roads and tracks acted as HSAs, but the majority of land areas adjacent to the open drainage channel network were not identified as HSAs (due to channelised runoff pathways or well drained

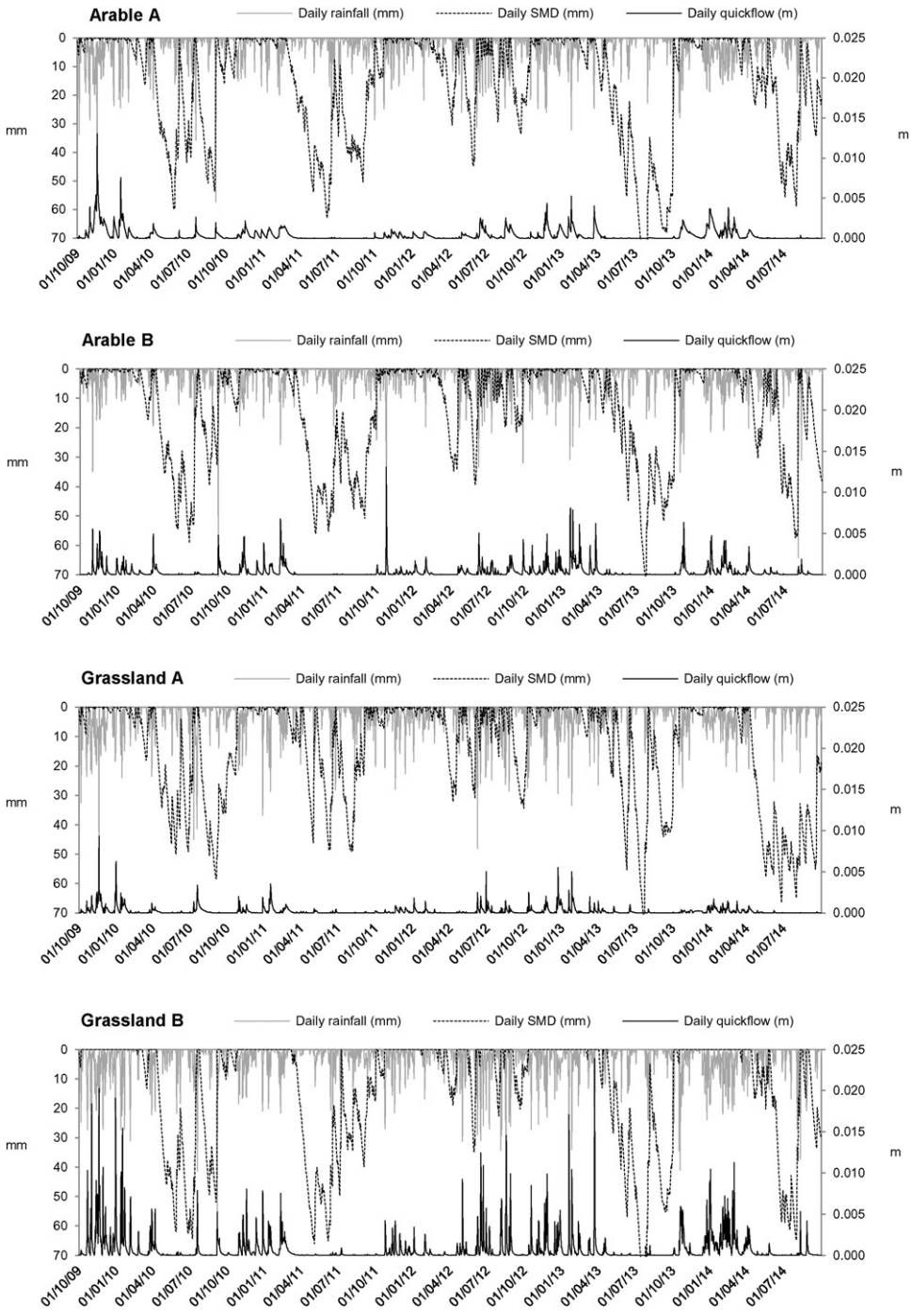

Fig. 5. Daily rainfall and quickflow events measured during 2009–2014 for each catchment, and SMD values (for well drained soils only).

soils). Bimodal distributions of HSA Index values in Fig. 4 and reductions in higher values compared to STI value distributions demonstrates the influence of flow sinks on impeding hydrological connectivity and HAAs in all catchments, particularly in Grassland A.

3.3. HSA Index validation

Distributions of the highest HSA Index values (Fig. 4) showed good agreement with the relative magnitude of rainfall-quickflow responses (Fig. 5) and HSA sizes (Table 2) in each of the four catchments. The largest, most hydrologically sensitive response to rainfall was predicted and observed in Grassland B, and then followed by Arable B. Arable A and Grassland A were predicted as the least sensitive, with similar HSA sizes, which was shown in the highest values of the HSA Index distributions. However, the raw rainfall-quickflow data (Fig. 5) indicated that Arable A had a slightly larger rainfall-quickflow response. This may be due a larger proportion of quickflow in this catchment being old water contributions to the ditch network, or the selected days used to estimate HSA sizes being a poorer representation of the whole population.

Correlation analysis showed that the size of HSAs predicted by HSA Index threshold values showed very good agreement with rainfall-quickflow derived HSA sizes, indicated by the closeness of the data to a 1:1 relationship (Fig. 4). Furthermore, a very strong positive relationship was shown between the inter-catchment differences in HSA sizes predicted by the HSA Index and the rainfall-quickflow data ($r = 0.92$). Although the STI also showed very strong agreement with rainfall-

Table 2
HSA sizes for each catchment, calculated using measured daily quickflow volumes (m^3) and rainfall depths (mm) during selected storm events under saturated conditions from 2009 to 2014.

		Daily rainfall (mm)	Daily quickflow (m^3)	HSA size (m^2)	HSA size (% of catchment)
Arable A	Min	2.8	38	10,175	0.1
	Max	57.2	21,527	683,132	6.2
	Mean	14.6	3715	215,014	1.9
	Q1	8.0	1003	75,387	0.7
	Median	11.7	1881	173,828	1.6
	Q3	19.2	5590	325,238	2.9
	Standard deviation	9.7	4260	154,874	1.4
	Standard error	1.3	559	20,336	0.2
	n	58			
Arable B	Min	2.6	189	35,403	0.4
	Max	35.0	65,961	2,141,581	22.8
	Mean	10.0	6126	398,789	4.3
	Q1	5.2	697	118,326	1.3
	Median	7.0	1633	283,464	3.0
	Q3	11.4	5293	509,739	5.4
	Standard deviation	8.1	12,665	416,857	4.4
	Standard error	1.2	1867	61,462	0.7
	n	46			
Grassland A	Min	1.2	19	15,446	0.2
	Max	48.0	38,131	1,141,653	15.1
	Mean	15.0	3723	216,739	2.9
	Q1	8.3	886	92,563	1.2
	Median	11.8	1788	140,060	1.9
	Q3	19.8	4137	239,890	3.2
	Standard deviation	9.5	5753	228,820	3.0
	Standard error	1.2	725	28,829	0.4
	n	63			
Grassland B	Min	1.7	126	46,386	0.4
	Max	64.2	93,133	2,255,024	19.1
	Mean	15.9	15,431	703,147	6.0
	Q1	9.0	2202	252,428	2.1
	Median	12.2	5983	401,850	3.4
	Q3	21.2	17,848	999,785	8.5
	Standard deviation	11.8	21,426	601,109	5.1
	Standard error	1.6	2971	83,359	0.7
	n	52			

quickflow derived HSA sizes, and inter-catchment differences showed very good correlation ($r = 0.92$), comparisons of the data with the 1:1 relationship indicates that it tends to overpredict HSA sizes (Fig. 4).

3.4. Cost implications for HSA targeting of mitigation measures

Proposed locations for targeting diffuse pollution mitigation measures at breakthrough and delivery points within HSAs are shown in Fig. 6b, with close-up examples shown in Fig. 7. In Arable A and Grassland A, the majority of locations were in lower hillslope positions adjacent to the open drainage channel network, although several locations were identified at breakthrough points along pathways which extended into upper hillslope positions. The high diffusivity of HSAs and pathways in Grassland B meant that targeted locations were found throughout the poorly drained soils at all hillslope positions. Delivery points were also identified throughout Arable B due to the high variability of both topography and soil drainage throughout the catchment.

The costs of targeted and blanket implementation of RBS for each margin width are shown in Table 4. Targeting RBS at delivery points within HSAs reduced costs compared to blanket implementation on average by €103,215 (66%) over 1 year and €616,077 (90%) over 5 years, based on 64 scenarios representing different RBS margin widths, LiDAR acquisition costs and the four study catchments of varying topography and soil drainage. The targeted approach also reduced potential RBS lengths in Arable A, Arable B, Grassland A and Grassland B by 97.4%, 96.8%, 94.6% and 97.3%, respectively.

Table 3
Total number of flow sinks for each catchment, total flow sink volume capacities, and proportions of HAAs and catchment areas which are hydrologically disconnected from the drainage channel network due to flow sinks during the UQ rainfall-quickflow event under saturated conditions.

	Arable A	Arable B	Grassland A	Grassland B
Total number of flow sinks with volume capacities ≥1 m^3	800	2487	1715	3101
Total flow sink volume capacity (m^3)	8298	24,389	29,445	59,584
Total flow sink volume capacity (equivalent number of Olympic size swimming pools (2500 m^3))	3.3	9.8	11.8	23.8
Total HAA area (m^2)	369,692	632,952	311,804	1,307,268
HAA area (m^2) that is hydrologically disconnected due to flow sinks	31,376	123,560	75,524	300,888
% of HAAs which are hydrologically disconnected	8.5	19.5	24.2	23.0
Proportion of HAAs that are HSAs (%)	91.5	80.5	75.8	77.0
Catchment area (m^2)	11,031,016	9,373,932	7,560,056	11,811,172
Flow sink upslope drainage area (m^2) that is hydrologically disconnected	1,851,780	2,584,228	2,527,868	2,938,368
% of catchment area which is hydrologically disconnected	16.8	27.6	33.4	24.9

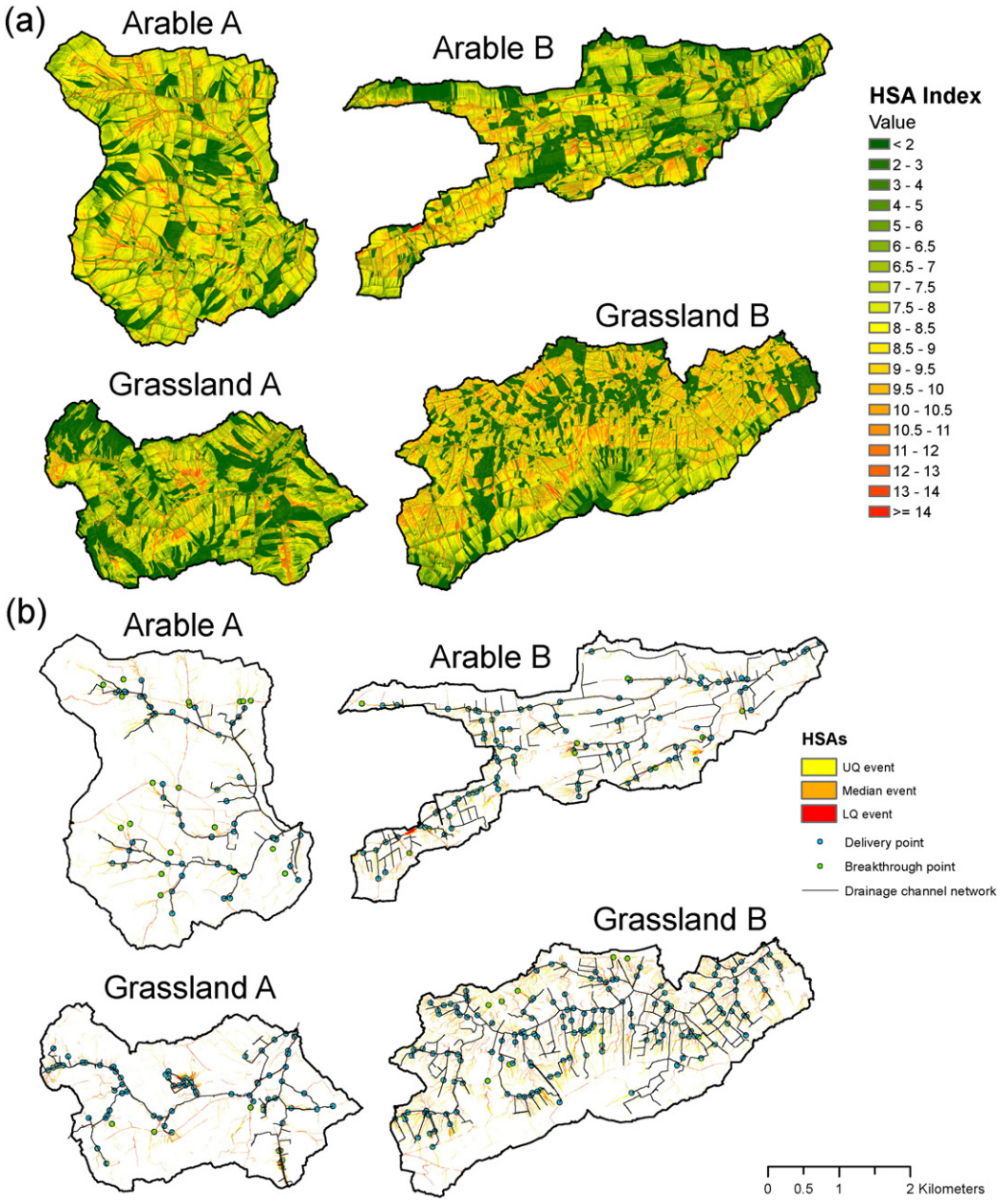

Fig. 6. Maps of the HSA Index (a) and HSAs (b) for each catchment. HSAs were delineated by selecting the catchment areas with the highest HSA Index values up to the threshold value which corresponded to LQ, median and UQ HSA sizes empirically estimated using rainfall-quickflow data. Also indicated are breakthrough points and delivery points at HSAs where mitigation measures could be targeted.

4. Discussion

4.1. The importance of flow sinks in mitigating pollutant transfers

Flow sinks were prolific throughout all study catchments (Fig. 4), and prevented significant proportions of HAAs and their upslope drainage areas from being hydrologically connected to the drainage network-i.e. a significant proportion were not HSAs (see Table 3). These features represent existing mitigation measures in the landscape that could attenuate diffuse pollutants and prevent delivery (Thomas et al., 2014; Schoumans et al., 2014). They should, therefore, be considered in mitigation strategies to avoid the unnecessary implementation of measures at these hydrologically disconnected HAAs. Furthermore, the removal of these depressions and hedgerow banks, which are particularly common across agricultural catchments in North West Europe, could reduce the size of hydrologically disconnected HAAs by 8.5–24.2% in this study. This could significantly increase surface runoff and associated risks to water quality, and as such these features should be preserved and enhanced.

4.2. Using the HSA Index to target and prioritise diffuse pollution mitigation measures

The HSA Index could improve the targeting of diffuse pollution mitigation measures compared to conventional topographic indices such as the TWI or STI, as it also identifies the HAAs that pose little risk of delivering pollutants. Furthermore, when using high resolution LiDAR DEMs, the HSA index can identify breakthrough points and delivery points that represent runoff-collecting-points and junctions of hydrological connectivity within and downslope of HSAs. The prevalence of microtopographic features (hedgerow banks) at field boundaries enhances mitigation potential, as multiple surface runoff pathways tend

Fig. 7. Close-up view of HSAs, breakthrough points (green), delivery points (blue), and flow sinks (grey).

to converge to single breakthrough points such as gateways or gaps in hedgerows at downslope field margins (Fig. 6b, Fig. 7). Similarly, the topography in much of Arable A and Grassland A tended to channelise and converge runoff generated from HSAs within a subcatchment to only a few downslope delivery points. These locations are, therefore, potentially the most cost-effective and unobtrusive for implementing mitigation measures if pollutant source pressures are either identified or, importantly, are likely to exist in future intensification scenarios. Conversely, hummocky and flatter topography in Grassland B and rolling-hillslopes in Arable B (Supplementary Fig. 1) tended to generate more sheet flow dynamics of overland flow, and larger diffusivity in HSAs and breakthrough and delivery points (Fig. 6). Such diffusivity hinders the potential to target mitigation measures close to pollutant sources (e.g. at breakthrough points), and in such areas it may be more cost-effective to target measures at delivery points only, or wider sections of the open drainage channel network. It should be noted, however, that identifying breakthrough and delivery points is a first step. The potential for implementation of mitigation options at these locations then needs to be discussed with farmers and landowners, especially in the context of farming operations.

This dialogue is important as the approaches and aims of mitigation at breakthrough and delivery points will differ, focusing on different stages of the pollutant transfer continuum. Measures targeted at breakthrough points would focus on reducing the transport and hydrological connectivity of pollutant transfer closer to the source in upper hillslope positions, via the interception and impediment of surface runoff. Additionally, measures targeted at delivery points would focus on preventing hydrological connectivity and pollutant delivery at the

Table 4
RBS costs for blanket and targeted implementation approaches for each margin width within an agri-environment scheme. RBS lengths were calculated along the whole drainage channel network for the blanket approach, and at HSA delivery points (identified using HSA maps derived from the HSA Index) for the targeted approach.

Catchment	Agri-environment scheme		Blanket approach			Targeted approach					RBS cost savings using targeted approach			
	Riparian margin (m width)	Payment rate (€/m/yr)	Total RBS length (m)	Total RBS cost (€/yr)	Total RBS cost (€/5 yr)	Total RBS length (m)	RBS cost (€/yr)	LiDAR acquisition cost (€)	Total RBS cost (€/yr)	Total RBS cost (€/5 yr)	Savings (€/yr)	Savings (%/yr)	Savings (€/5 yr)	Savings (%/5 yr)
Arable A	3	0.9	41,910	37,719	188,595	1110	999	10,000	10,999	14,995	26,720	71	173,600	92
								20,000	20,999	24,995	16,720	44	163,600	87
								30,000	30,999	34,995	6720	18	153,600	81
								40,000	40,999	44,995	−3280	−9	143,600	76
	6	1.2	41,910	50,292	251,460	1110	1332	10,000	11,332	16,660	38,960	77	234,800	93
								20,000	21,332	26,660	28,960	58	224,800	89
								30,000	31,332	36,660	18,960	38	214,800	85
								40,000	41,332	46,660	8960	18	204,800	81
	10	1.6	41,910	67,056	335,280	1110	1776	10,000	11,776	18,880	55,280	82	316,400	94
								20,000	21,776	28,880	45,280	68	306,400	91
								30,000	31,776	38,880	35,280	53	296,400	88
								40,000	41,776	48,880	25,280	38	286,400	85
	30	3.6	41,910	150,876	754,380	1110	3996	10,000	13,996	29,980	136,880	91	724,400	96
								20,000	23,996	39,980	126,880	84	714,400	95
								30,000	33,996	49,980	116,880	77	704,400	93
								40,000	43,996	59,980	106,880	71	694,400	92
Arable B	3	0.9	82,874	74,587	372,933	2645	2381	10,000	12,381	21,903	62,206	83	351,031	94
								20,000	22,381	31,903	52,206	70	341,031	91
								30,000	32,381	41,903	42,206	57	331,031	89
								40,000	42,381	51,903	32,206	43	321,031	86
	6	1.2	82,874	99,449	497,244	2645	3174	10,000	13,174	25,870	86,275	87	471,374	95
								20,000	23,174	35,870	76,275	77	461,374	93
								30,000	33,174	45,870	66,275	67	451,374	91
								40,000	43,174	55,870	56,275	57	441,374	89
	10	1.6	82,874	132,598	662,992	2645	4232	10,000	14,232	31,160	118,366	89	631,832	95
								20,000	24,232	41,160	108,366	82	621,832	94
								30,000	34,232	51,160	98,366	74	611,832	92
								40,000	44,232	61,160	88,366	67	601,832	91
	30	3.6	82,874	298,346	1,491,732	2645	9522	10,000	19,522	57,610	278,824	93	1,434,122	96
								20,000	29,522	67,610	268,824	90	1,424,122	95
								30,000	39,522	77,610	258,824	87	1,414,122	95
								40,000	49,522	87,610	248,824	83	1,404,122	94
Grassland A	3	0.9	40,182	36,164	180,819	2155	1940	10,000	11,940	19,698	24,224	67	161,122	89
								20,000	21,940	29,698	14,224	39	151,122	84
								30,000	31,940	39,698	4224	12	141,122	78
								40,000	41,940	49,698	−5776	−16	131,122	73
	6	1.2	40,182	48,218	241,092	2155	2586	10,000	12,586	22,930	35,632	74	218,162	90
								20,000	22,586	32,930	25,632	53	208,162	86
								30,000	32,586	42,930	15,632	32	198,162	82
								40,000	42,586	52,930	5632	12	188,162	78
	10	1.6	40,182	64,291	321,456	2155	3448	10,000	13,448	27,240	50,843	79	294,216	92
								20,000	23,448	37,240	40,843	64	284,216	88
								30,000	33,448	47,240	30,843	48	274,216	85
								40,000	43,448	57,240	20,843	32	264,216	82
	30	3.6	40,182	144,655	723,276	2155	7758	10,000	17,758	48,790	126,897	88	674,486	93
								20,000	27,758	58,790	116,897	81	664,486	92
								30,000	37,758	68,790	106,897	74	654,486	90
								40,000	47,758	78,790	96,897	67	644,486	89
Grassland B	3	0.9	125,322	112,790	563,949	3358	3022	10,000	13,022	25,111	99,768	88	538,838	96
								20,000	23,022	35,111	89,768	80	528,838	94
								30,000	33,022	45,111	79,768	71	518,838	92
								40,000	43,022	55,111	69,768	62	508,838	90
	6	1.2	125,322	150,386	751,932	3358	4030	10,000	14,030	30,148	136,357	91	721,784	96
								20,000	24,030	40,148	126,357	84	711,784	95
								30,000	34,030	50,148	116,357	77	701,784	93
								40,000	44,030	60,148	106,357	71	691,784	92
	10	1.6	125,322	200,515	1,002,576	3358	5373	10,000	15,373	36,864	185,142	92	965,712	96
								20,000	25,373	46,864	175,142	87	955,712	95
								30,000	35,373	56,864	165,142	82	945,712	94
								40,000	45,373	66,864	155,142	77	935,712	93
	30	3.6	125,322	451,159	2,255,796	3358	12,089	10,000	22,089	70,444	429,070	95	2,185,352	97
								20,000	32,089	80,444	419,070	93	2,175,352	96
								30,000	42,089	90,444	409,070	91	2,165,352	96
								40,000	52,089	100,444	399,070	88	2,155,352	96
Average			72,572	132,444	662,220	2317	4229		29,229	46,143	103,215	66	616,077	90

drainage network in lower hillslope positions. This constitutes a catchment 'treatment-train' approach to runoff and pollutant transfer pathways at both breakthrough and delivery points (e.g. Ferrier et al., 2005; Bastien et al., 2010). For example, various precisely targeted measures at breakthrough points could include depressions and hedgerows (Schoumans et al., 2014), runoff attenuating features (Wilkinson et al., 2014), relocation of gateways, and sediment and nutrient traps (USEPA, 1993). Targeted delivery point measures along the 'treatment-train' could include RBS (Tomer et al., 2003), small field wetlands (Ockenden et al., 2014), permeable reactive interceptors (Fenton et al., 2014), rural sustainable drainage systems (Environment Agency, 2012) and the modification of open ditch geometry (Shore et al., 2015).

Targeting measures at breakthrough and delivery points can be prioritised to further improve cost-effectiveness. Breakthrough and delivery points with the highest HSA Index values should become hydrologically active more frequently (e.g. during LQ or median storm events), and thus should be prioritised, whereas those with slightly lower values will only become hydrologically active during more intense or prolonged (UQ) events. However, hydrologically sensitive moments during these largest events are when the greatest pollutant transfers occur (Archibald et al., 2014), and as such implementing mitigation measures at such locations should not be dismissed. Nevertheless, results suggest that the most extreme hydrologically sensitive moments in Arable B and Grassland A and B may be very difficult to mitigate, as maximum HSA sizes represented 15.1–22.8% of the catchment area (Table 2). Another approach for prioritising measures is upslope HSA size, as points with larger upslope HSAs should experience greater runoff volumes and potential for pollutant transport (see Fig. 6). The design of measures at high-priority points must, therefore, account for increased runoff frequencies and volumes. Runoff volumes can be calculated using upslope HSA size and rainfall depths similar to the methodology used in Supplementary Fig. 2. Finally, mitigation measures could be focused on sections of the open drainage channel network at highest hydrological sensitivity and risk of pollutant delivery, identified as those with a greater number of delivery points or high priority points (e.g. Fenton et al., 2014; Shore et al., 2015).

4.3. HSA Index application and further development

In addition to being a realistic hydrological transport component if used in a fully evolved CSA Index or model, the HSA Index could be used to encourage the uptake of mitigation measures such as targeted RBS by farmers within agri-environmental or species conservation schemes. This is especially pertinent in those agricultural catchments where hydrological transport and connectivity is an overwhelming component in the pollutant transfer continuum from soil surfaces (Thompson et al., 2012), or where agricultural intensification is planned which could substantially increase source and land management pressures. Results here indicate that the HSA approach would considerably reduce RBS implementation costs by significantly reducing the amount of agricultural land that would be taken out of production compared to blanket implementation (Table 4). It would also minimise the disturbance of agricultural practices as breakthrough and delivery points are unobtrusive locations within edge-of-field margins. These are key concerns that currently dissuade farmers from adopting RBS (Buckley, 2012; Buckley et al., 2012). For example, of approximately 27,000 farmers in Tranche 1 of GLAS in Ireland, only 101 applied for RBS margins; 11, 5, 9 and 76 for RBS margins of 3, 6, 9 and 30 m, respectively (Department of Agriculture, Food and the Marine, pers comm). This follows very low uptake in previous agri-environmental schemes in Ireland (Carlin et al., 2010). As the efficacy of RBS in reducing pollutant transfers increases with wider margins (Zhang et al., 2010; Hoffmann et al., 2009; Schmitt et al., 1999), encouraging the adoption of wider RBS margins through a targeted approach is important. Other studies also demonstrate the improved cost-effectiveness likely with a targeted approach (e.g. Qiu and Dosskey, 2012; Doody et al., 2012, Ó hUallacháin, 2014).

To more accurately model temporal variations in HSA extents, the HSA Index could be fully integrated with a SMD model (e.g. Schulte et al., 2005) and rainfall data, similar to approaches by Dahlke et al. (2013), Schneiderman et al. (2007) and Archibald et al. (2014). This would be particularly useful for identifying hydrologically sensitive moments (i.e. runoff forecasting) and informing best management practices such as temporary restrictions to fertiliser applications to reduce incidental losses. This approach would thus account for differences in rainfall frequency and intensity between catchment locations and hence differences in the hydrological activity of HSAs.

5. Conclusions

An essential component of CSA models used to manage diffuse pollution in agricultural catchments is a realistic representation of hydrological transport. This need is even greater in catchments where hydrological transport has a predominant control in pollutant transfers. In this study, HSAs were defined at the sub-field scale, and took into account the effects of flow sinks on hydrological connectivity from soil surfaces to the open-channel network. LiDAR DEMs at a fine scale resolution (0.25–2 m), combined with soil hydraulic properties to give an overall Soil Topographic Index, was the framework for defining a HSA Index, and this is the recommended scale for defining these risk assessments at sub-field scale.

Analysis of rainfall-quickflow patterns indicated that HSAs ranged from 1.6–3.4% of the catchment area during median storm events and 2.9–8.5% during upper quartile events depending on whether well or poorly drained soils dominated. These HSA sizes showed very strong agreement with the predictions of HSA sizes derived from HSA Index threshold values, and strong positive relationships between inter-catchment differences were found ($r = 0.92$).

Results showed that flow sinks were widespread throughout all catchments and caused 8.5–24.2% of HAAs and 16.8–33.4% of catchment areas to become hydrologically disconnected from the open drainage channel network. Without considering these runoff-attenuating-features, diffuse pollutant mitigation measures would be unnecessarily implemented.

Furthermore, the identification of 'breakthrough' and 'delivery' points on HSA maps facilitates a catchment 'treatment-train' approach, which precisely targets different mitigation measures along the pollutant transfer continuum. This kind of approach is likely to reduce the amount of land deemed necessary for diffuse pollution measures. For example, in this study, the potential implementation costs of riparian buffer strips were reduced in scenario agri-environmental schemes by 66% and 90% over 1 and 5 years, respectively, due to an average decrease in RBS lengths of 96.8%.

In addition to being able to provide a sub-field scale transport component within a fully evolved CSA model, the HSA approach defined here has the potential to be used to pre-empt or to offset the increase in source pressures that might occur due to land use intensification, especially in catchments dominated by surface runoff pathways. Using available LiDAR and soils data, the approach, therefore, is suited as a tool to support sustainable agricultural intensification.

Supplementary data to this article can be found online at http://dx.doi.org/10.1016/j.scitotenv.2016.02.183.

Acknowledgements

This research is part of the Agricultural Catchments Programme (ACP), funded by the Irish Department of Agriculture, Food and the Marine (DAFM) and the Teagasc Walsh Fellowship Scheme (DAFM 6300). We thank ACP farmers for cooperation and access to their land, the ACP team and staff at the Teagasc Environment, Soils and Land Use Department, Johnstown Castle, Wexford, Ireland. We also thank the Irish

DAFM for discussions on the applicability of topographic indices within policy, and acknowledge FugroBKS Ltd., Coleraine, N. Ireland, for acquisition of the LiDAR data.

References

Agnew, L.J., Lyon, S., Gerard-Marchant, P., Collins, V.B., Lembo, A.J., Steenhuis, T.S., Walter, M.T., 2006. Identifying hydrologically sensitive areas: bridging the gap between science and application. J. Environ. Manag. 78, 63–76.

Archibald, J.A., Buchanan, B.P., Fuka, D.R., Georgakakos, C.B., Lyon, S.W., Walter, M.T., 2014. A simple, regionally parameterized model for predicting nonpoint source areas in the northeastern US. Journal of Hydrology: Regional Studies 1, 74–91.

Bastien, N., Arthur, S., Wallis, S., Scholz, M., 2010. The best management of SuDS treatment trains: a holistic approach. Water Science & Technology 61, 263–272.

Beven, K.J., Kirkby, M.J., 1979. A physically based, variable contributing area model of basin hydrology. Hydrol. Sci. Bull. 24, 43–69.

Buchanan, B.P., Fleming, M., Schneider, R.L., Richards, B.K., Archibald, J., Qiu, Z., Walter, M.T., 2014. Evaluating topographic wetness indices across central New York agricultural landscapes. Hydrol. Earth Syst. Sci. 18, 3279–3299.

Buckley, C., 2012. Implementation of the EU Nitrates Directive in the Republic of Ireland — a view from the farm. Ecol. Econ. 78, 29–36.

Buckley, C., Hynes, S., Mechan, S., 2012. Supply of an ecosystem service—farmers' willingness to adopt riparian buffer zones in agricultural catchments. Environ. Sci. Pol. 24, 101–109.

Buda, A.R., Kleinman, P.J.A., Srinivasan, M.S., Bryant, R.B., Feyereisen, G.W., 2009. Effects of hydrology and field management on phosphorus transport in surface runoff. J. Environ. Qual. 38, 2273–2284.

Campbell, J., Jordan, P., Arnscheidt, J., 2015. Using high-resolution phosphorus data to investigate mitigation measures in headwater river catchments. Hydrol. Earth Syst. Sci. 19, 453–464.

Carlin, C., Gormally, M., Ó Huallacháin, D., Finn, J., 2010. Experts assessments of biodiversity options and supplementary measures in REPS 4. Report for Department of Agriculture, Food and the Marine.

Creamer, R., Simo, I., Reidy, B., Carvalho, J., Fealy, R.M., Hallett, S., Jones, R., Holden, A., Holden, N., Hannam, J., Massey, P., Mayr, T., Mcdonald, E., O'rourke, S., Sills, P., Truckell, I., Zawadzka, J., Schulte, R.P.O., 2014. Irish Soil Information System—Synthesis Report. Teagasc Environment Research Centre, Johnstown Castle, Wexford, Co. Wexford, Ireland.

DAFM, 2015. Green, Low-carbon, Agri-environment Scheme (GLAS) Specification for Tranche 1 Participants, 18th September 2015. DAFM, Dublin.

Dahlke, H., Easton, Z., Fuka, D., Walter, M., Steenhuis, T., 2013. Real-Time Forecast of Hydrologically Sensitive Areas in the Salmon Creek Watershed, New York State, Using an Online Prediction Tool. Water 5, 917.

Daniel, T.C., Sharpley, A.N., Lemunyon, J.L., 1998. Agricultural phosphorus and eutrophication: a symposium overview. J. Environ. Qual. 27, 251–257.

Djodjic, F., Villa, A., 2015. Distributed, high-resolution modelling of critical source areas for erosion and phosphorus losses. Ambio 44, 241–251.

Doody, D.G., Archbold, M., Foy, R.H., Flynn, R., 2012. Approaches to the implementation of the Water Framework Directive: targeting mitigation measures at critical source areas of diffuse phosphorus in Irish catchments. J. Environ. Manag. 93, 225–234.

Environment Agency, 2012. Rural Sustainable Drainage Systems. Environment Agency, Horizon House, Deanery Road, Bristol, BS1 5AH.

Fenton, O., Schulte, R.P., Jordan, P., Lalor, S.T., Richards, K.G., 2011. Time lag: a methodology for the estimation of vertical and horizontal travel and flushing timescales to nitrate threshold concentrations in Irish aquifers. Environ. Sci. Pol. 14, 419–431.

Fenton, O., Healy, M., Brennan, F., Jahangir, M., Lanigan, G., Richards, K., Thornton, S., Ibrahim, T., 2014. Permeable reactive interceptors: blocking diffuse nutrient and greenhouse gases losses in key areas of the farming landscape. J. Agric. Sci. 152, 71–81.

Ferrier, R.C., D'arcy, B.J., Macdonald, J., Aitken, M., 2005. Diffuse pollution—what is the nature of the problem? Water and Environment Journal 19, 361–366.

Galzki, J.C., Birr, A.S., Mulla, D.J., 2011. Identifying critical agricultural areas with three-meter LiDAR elevation data for precision conservation. J. Soil Water Conserv. 66, 423–430.

Gburek, W.J., Sharpley, A.N., Heathwaite, L., Folmar, G.J., 2000. Phosphorus management at the watershed scale: a modification of the phosphorus index. J. Environ. Qual. 29, 130–144.

Hahn, C., Prasuhn, V., Stamm, C., Milledge, D.G., Schulin, R., 2014. A comparison of three simple approaches to identify critical areas for runoff and dissolved reactive phosphorus losses. Hydrol. Earth Syst. Sci. 18, 2975–2991.

Haygarth, P.M., Condron, L.M., Heathwaite, A.L., Turner, B.L., Harris, G.P., 2005. The phosphorus transfer continuum: linking source to impact with an interdisciplinary and multi-scaled approach. Sci. Total Environ. 344, 5–14.

Heckrath, G., Bechmann, M., Ekholm, P., Ulén, B., Djodjic, F., Andersen, H.E., 2008. Review of indexing tools for identifying high risk areas of phosphorus loss in Nordic catchments. J. Hydrol. 349, 68–87.

Hoffmann, C.C., Kjaergaard, C., Uusi-Kämppä, J., Hansen, H.C.B., Kronvang, B., 2009. Phosphorus retention in riparian buffers: review of their efficiency. J. Environ. Qual. 38, 1942–1955.

Jarvie, H.P., Sharpley, A.N., Withers, P.J.A., Scott, J.T., Haggard, B.E., Neal, C., 2013. Phosphorus mitigation to control river eutrophication: murky waters, inconvenient truths, and "postnormal" science. J. Environ. Qual. 42, 295–304.

Jenson, S.K., Domingue, J.O., 1988. Extracting topographic structure from digital elevation data for geographic information system analysis. Photogramm. Eng. Remote. Sens. 54, 1593–1600.

Jordan, P., Melland, A.R., Mellander, P.E., Shortle, G., Wall, D., 2012. The seasonality of phosphorus transfers from land to water: implications for trophic impacts and policy evaluation. Sci. Total Environ. 434, 101–109.

Kleinman, P., Sharpley, A.N., Buda, A., Mcdowell, R., Allen, A., 2011. Soil controls of phosphorus in runoff: management barriers and opportunities. Can. J. Soil Sci. 91, 329–338.

Lane, S.N., Reaney, S.M., Heathwaite, A.L., 2009. Representation of landscape hydrological connectivity using a topographically driven surface flow index. Water Resour. Res. 45, W08423.

Lemunyon, J.L., Gilbert, R.G., 1993. The concept and need for a phosphorus assessment tool. J. Prod. Agric. 6, 483–486.

Li, S., Macmillan, R.A., Lobb, D.A., Mcconkey, B.G., Moulin, A., Fraser, W.R., 2011. Lidar DEM error analyses and topographic depression identification in a hummocky landscape in the prairie region of Canada. Geomorphology 129, 263–275.

Lindsay, J.B., Creed, I.F., 2006. Distinguishing actual and artefact depressions in digital elevation data. Comput. Geosci. 32, 1192–1204.

Marjerison, R.D., Dahlke, H., Easton, Z.M., Seifert, S., Walter, M.T., 2011. A Phosphorus Index transport factor based on variable source area hydrology for New York State. J. Soil Water Conserv. 66, 149–157.

Maune, D.F., Kopp, S.M., Crawford, C.A., Zervas, C.E., 2007. Introduction: Digital Elevation Models, Digital Elevation Model Technologies and Applications: The DEM Users Manual. second ed. American Society for Photogrammetry and Remote Sensing, Maryland.

Mcdowell, R.W., Nash, D., 2012. A review of the cost-effectiveness and suitability of mitigation strategies to prevent phosphorus loss from dairy farms in New Zealand and Australia. J. Environ. Qual. 41, 680–693.

Mellander, P.-E., Melland, A.R., Jordan, P., Wall, D.P., Murphy, P.N.C., Shortle, G., 2012. Quantifying nutrient transfer pathways in agricultural catchments using high temporal resolution data. Environ. Sci. Pol. 24, 44–57.

Mellander, P.-E., Jordan, P., Shore, M., Melland, A.R., Shortle, G., 2015. Flow paths and phosphorus transfer pathways in two agricultural streams with contrasting flow controls. Hydrol. Process. 29, 3504–3518.

Murphy, P., Mellander, P.-E., Melland, A., Buckley, C., Shore, M., Shortle, G., Wall, D., Treacy, M., Shine, O., Mechan, S., 2015. Variable response to phosphorus mitigation measures across the nutrient transfer continuum in a dairy grassland catchment. Agric. Ecosyst. Environ. 207, 192–202.

Needelman, B.A., Gburek, W.J., Petersen, G.W., Sharpley, A.N., Kleinman, P.J.A., 2004. Surface runoff along two agricultural hillslopes with contrasting soils. Soil Sci. Soc. Am. J. 68, 914–923.

Ockenden, M.C., Deasy, C., Quinton, J.N., Surridge, B., Stoate, C., 2014. Keeping agricultural soil out of rivers: evidence of sediment and nutrient accumulation within field wetlands in the UK. J. Environ. Manag. 135, 54–62.

Ó hUallacháin, D., 2014. Wider riparian buffer strips: a cost-effective conservation measure for freshwater pearl mussels in Ireland? Biology and Environment: Proceedings of the Royal Irish Academy 114B, 101–107.

Petroselli, A., 2012. LIDAR data and hydrological applications at the basin scale. GIScience & Remote Sensing 49, 139–162.

Pionke, H.B., Gburek, W.J., Sharpley, A.N., 2000. Critical source area controls on water quality in an agricultural watershed located in the Chesapeake Basin. Ecol. Eng. 14, 325–335.

Qiu, Z., 2003. A VSA-based strategy for placing conservation buffers in agricultural watersheds. Environ. Manag. 32, 299–311.

Qiu, Z., Dosskey, M.G., 2012. Multiple function benefit — cost comparison of conservation buffer placement strategies. Landsc. Urban Plan. 107, 89–99.

Quinn, P., Beven, K., Chevallier, P., Planchon, O., 1991. The prediction of hillslope flow paths for distributed hydrological modelling using digital terrain models. Hydrol. Process. 5, 59–79.

Reidy, B., Simo, I., Sills, P., Creamer, R.E., 2016. Pedotransfer functions for Irish soils — estimation of bulk density (ρb) per horizon type. Soil 2, 25–39.

Schmitt, T., Dosskey, M., Hoagland, K., 1999. Filter strip performance and processes for different vegetation, widths, and contaminants. J. Environ. Qual. 28, 1479–1489.

Schneiderman, E.M., Steenhuis, T.S., Thongs, D.J., Easton, Z.M., Zion, M.S., Neal, A.L., Mendoza, G.F., Todd Walter, M., 2007. Incorporating variable source area hydrology into a curve-number-based watershed model. Hydrol. Process. 21, 3420–3430.

Schoumans, O., Chardon, W., Bechmann, M., Gascuel-Odoux, C., Hofman, G., Kronvang, B., Rubæk, G.H., Ulen, B., Dorioz, J.-M., 2014. Mitigation options to reduce phosphorus losses from the agricultural sector and improve surface water quality: a review. Sci. Total Environ. 468, 1255–1266.

Schulte, R., Diamond, J., Finkele, K., Holden, N., Brereton, A., 2005. Predicting the soil moisture conditions of Irish grasslands. Irish Journal of Agricultural and Food Research 95–110.

Sharpley, A.N., Weld, J.L., Beegle, D.B., Kleinman, P.J.A., Gburek, W.J., Moore, P.A., Mullins, G., 2003. Development of phosphorus indices for nutrient management planning strategies in the United States. J. Soil Water Conserv. 58, 137–152.

Sharpley, A.N., Kleinman, P.J., Flaten, D.N., Buda, A.R., 2011. Critical source area management of agricultural phosphorus: experiences, challenges and opportunities. Water Sci. Technol. 64, 945–952.

Sharpley, A., Bolster, C., Conover, C., Dayton, E., Davis, J., Easton, Z., Good, L., Gross, C., Kleinman, P., Mallinaro, A., 2013. Technical Guidance for Assessing Phosphorus Indices.

Sherriff, S.C., Rowan, J.S., Melland, A.R., Jordan, P., Fenton, O., Huallacháin, Ó., 2015. Investigating suspended sediment dynamics in contrasting agricultural catchments using ex situ turbidity-based suspended sediment monitoring. Hydrol. Earth Syst. Sci. 19, 3349–3363.

Shore, M., Murphy, P.N.C., Jordan, P., Mellander, P.E., Kelly-Quinn, M., Cushen, M., Mechan, S., Shine, O., Melland, A.R., 2013. Evaluation of a surface hydrological connectivity index in agricultural catchments. Environ. Model Softw. 47, 7–15.

Shore, M., Jordan, P., Mellander, P.E., Kelly-Quinn, M., Wall, D.P., Murphy, P.N.C., Melland, A.R., 2014. Evaluating the critical source area concept of phosphorus loss from soils to water-bodies in agricultural catchments. Sci. Total Environ. 490, 405–415.

Shore, M., Jordan, P., Mellander, P.E., Kelly-Quinn, M., Melland, A.R., 2015. An agricultural drainage channel classification system for phosphorus management. Agric. Ecosyst. Environ. 199, 207–215.

Srinivasan, M., Mcdowell, R., 2007. Hydrological approaches to the delineation of critical-source areas of runoff. N. Z. J. Agric. Res. 50, 249–265.

Srinivasan, M.S., Mcdowell, R.W., 2009. Identifying critical source areas for water quality: 1. Mapping and validating transport areas in three headwater catchments in Otago, New Zealand. J. Hydrol. 379, 54–67.

Tarboton, D.G., 1997. A new method for the determination of flow directions and upslope areas in grid digital elevation models. Water Resour. Res. 33, 309–319.

Thomas, I., Jordan, P., Shine, O., Fenton, O., Mellander, P.-E., Dunlop, P., Murphy, P.N.C., 2014. Comparing high resolution LiDAR and conventional digital elevation models for identifying potential phosphorus transfer pathways. Presented at the ASA, CSSA and SSSA 2014 Annual Meeting, 2nd–5th November, Long Beach, CA, USA.

Thompson, J.J.D., Doody, D.G., Flynn, R., Watson, C.J., 2012. Dynamics of critical source areas: does connectivity explain chemistry? Sci. Total Environ. 435–436, 499–508.

Tomer, M.D., James, D.E., Isenhart, T.M., 2003. Optimizing the placement of riparian practices in a watershed using terrain analysis. J. Soil Water Conserv. 58, 198–206.

Ulén, B., Bechmann, M., Fölster, J., Jarvie, H.P., Tunney, H., 2007. Agriculture as a phosphorus source for eutrophication in the north-west European countries, Norway, Sweden, United Kingdom and Ireland: a review. Soil Use Manag. 23, 5–15.

USEPA, 1993. Guidance Specifying Management Measures for Sources of Nonpoint Pollution in Coastal Waters. EPA 840-B-92-002. U.S. Environmental Protection Agency, Office of Water, Washington, DC.

Valle Junior, R.F., Varandas, S.G.P., Sanches Fernandes, L.F., Pacheco, F.A.L., 2014. Environmental land use conflicts: a threat to soil conservation. Land Use Policy 41, 172–185.

van Genuchten, M., Leij, F., Yates, S., 1991. The RETC Code for Quantifying the Hydraulic Functions of Unsaturated Soils. Version 1.0 EPA Report 600/2–91/065. U.S. Salinity Laboratory, USDA-ARS, Riverside, California.

Vaze, J., Teng, J., Spencer, G., 2010. Impact of DEM accuracy and resolution on topographic indices. Environ. Model Softw. 25, 1086–1098.

Wall, D., Jordan, P., Melland, A.R., Mellander, P.E., Buckley, C., Reaney, S.M., Shortle, G., 2011. Using the nutrient transfer continuum concept to evaluate the European Union Nitrates Directive National Action Programme. Environ. Sci. Pol. 14, 664–674.

Walter, M.T., Walter, M.F., Brooks, E.S., Steenhuis, T.S., Boll, J., Weiler, K., 2000. Hydrologically sensitive areas: variable source area hydrology implications for water quality risk assessment. J. Soil Water Conserv. 55, 277–284.

Walter, M.T., Steenhuis, T.S., Mehta, V.K., Thongs, D., Zion, M., Schneiderman, E., 2002. Refined conceptualization of TOPMODEL for shallow subsurface flows. Hydrol. Process. 16, 2041–2046.

Wang, L., Liu, H., 2006. An efficient method for identifying and filling surface depressions in digital elevation models for hydrologic analysis and modelling. Int. J. Geogr. Inf. Sci. 20, 193–213.

Wechsler, S.P., 2007. Uncertainties associated with digital elevation models for hydrologic applications: a review. Hydrological Earth System Sciences 11, 1481–1500.

White, M.J., Arnold, J.G., 2009. Development of a simplistic vegetative filter strip model for sediment and nutrient retention at the field scale. Hydrol. Process. 23, 1602–1616.

Wilkinson, M.E., Quinn, P.F., Barber, N.J., Jonczyk, J., 2014. A framework for managing runoff and pollution in the rural landscape using a Catchment Systems Engineering approach. Sci. Total Environ. 468–469, 1245–1254.

Zevenbergen, L.W., Thorne, C.R., 1987. Quantitative analysis of land surface topography. Earth Surf. Process. Landf. 12, 47–56.

Zhang, X., Liu, X., Zhang, M., Dahlgren, R.A., Eitzel, M., 2010. A review of vegetated buffers and a meta-analysis of their mitigation efficacy in reducing nonpoint source pollution. J. Environ. Qual. 39, 76–84.